nature communications

Article

https://doi.org/10.1038/s41467-025-59541-4

# Nickel-embedded three-in-one pyridyl-quinoline-linked covalent organic framework photocatalysts for universal C($sp^2$) cross-coupling reactions

Received: 24 March 2025

Accepted: 28 April 2025

Published online: 21 May 2025

Check for updates

A list of authors and their affiliations appears at the end of the paper

Metallaphotocatalysis, integrating interlocked photocatalytic cycles and transition-metal catalysis, harmonizes the ground state and excited state reactivities, enabling cross-couplings under mild conditions and expanding the scope of accessible transformations. However, homogeneous dual metallaphotocatalysts often suffer from limitations such as low catalyst stability, high metal loading, and challenges in catalyst recycling. In this study, we engineered a class of nickel-incorporated pyridyl-quinoline-linked covalent organic frameworks (Ni-PQCOFs) serving as robust and efficient heterogeneous metallaphotocatalysts. These Ni-PQCOFs facilitate universal visible-light-driven C($sp^2$)-carbon and heteroatom (S, N, O, B, P, Se, and Cl) bond formations across a broad range of aromatic halides and nucleophiles, while maintaining low metal loading (1-2 mol%). The Ni-PQCOFs, featuring fully conjugated and tunable pyridyl-quinoline (PQ) motifs, exhibit exceptional (photo)chemical stability, broadened absorption wavelength range, and enhanced redox capability. Remarkably, these COF-based heterogeneous metallaphotocatalysts exhibited significantly enhanced catalytic efficiency compared to their homogeneous counterparts. The versatility and practicality of this photocatalytic system extend to diverse synthetic applications, including late-stage functionalization of complex molecules, sequential functionalizations, and decagram-scale synthesis assisted by an in-house-built high-speed circulation flow system. Moreover, the micrometer-sized Ni-PQCOF catalyst could be recycled over 10 times through direct filtration with minimal activity loss and negligible metal leaching. All these advantages establish Ni-PQCOFs as versatile, effective, and sustainable metallaphotocatalysts for cross-coupling reactions.

Metallaphotocatalysis-enabled cross-coupling reactions, with interlocked photocatalysis and transition-metal catalysis, have revolutionized the landscape of organic synthesis by facilitating the formation of a diverse array of carbon-carbon and carbon-heteroatom bonds under mild conditions (Fig. 1a)[1–6]. Despite their impressive synthetic capabilities, homogeneous metallaphotocatalytic systems encounter several challenges, including low catalyst stability (e.g., labile structure towards radicals, metal aggregation into nanoparticles), high metal

e-mail: chmjie@nus.edu.sg

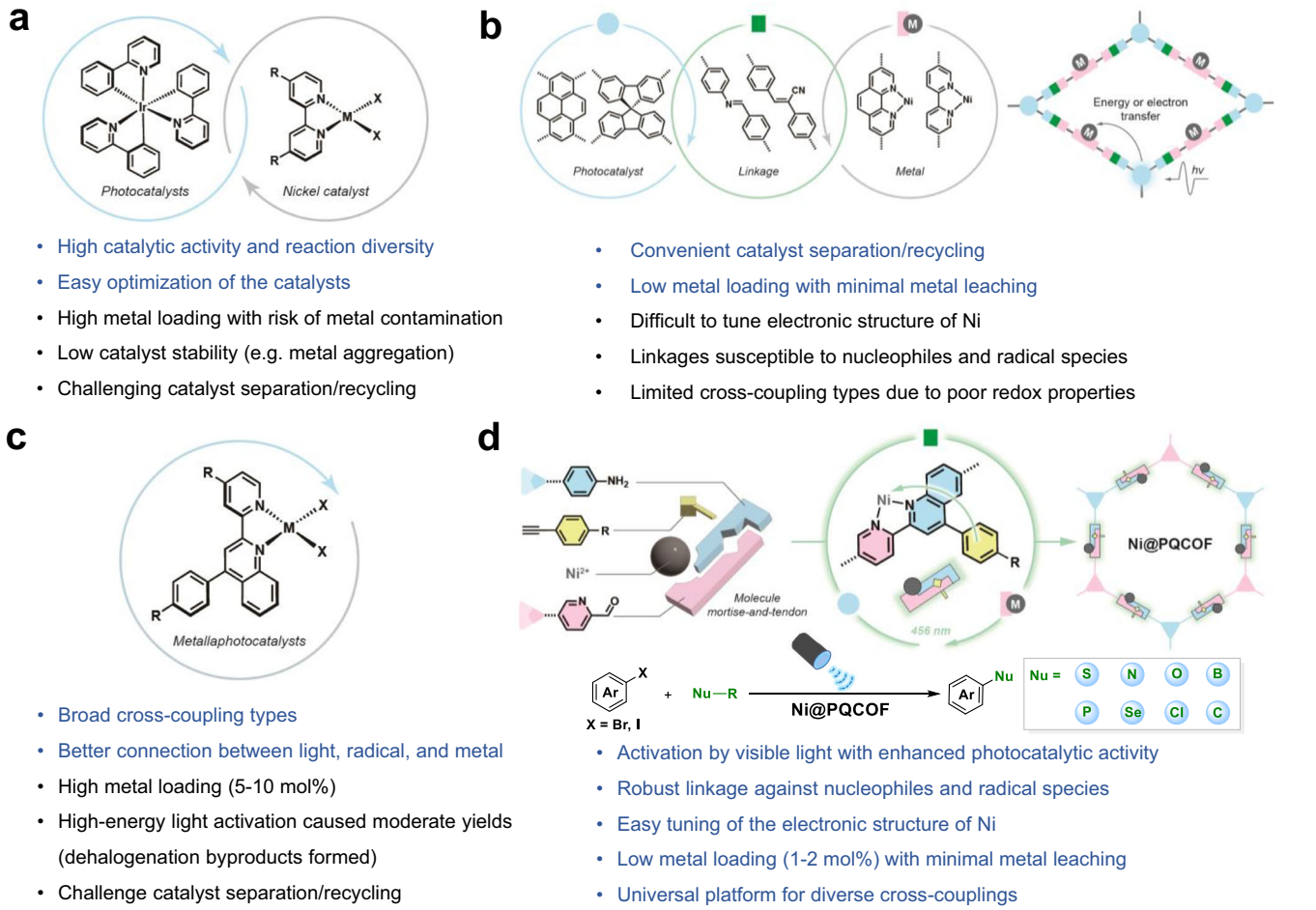


**Fig. 1 | Development of metallaphotocatalytic cross-couplings. a** State-of-the-art homogeneous dual metallaphotocatalysts for cross-couplings. **b** COF-based dual metallaphotocatalysts for cross-coupling reactions. **c** Two-in-one homogeneous metallaphotocatalysts. **d** This work: three-in-one pyridyl-quinoline-linked COFs for universal cross-couplings.

loading, difficulties in product separation and purification, and catalyst recycling[7]. To address these limitations, the development of heterogeneous metallaphotocatalysts presents a promising avenue, by enabling straightforward catalyst separation and recovery. While semiconductive materials like carbon dots[8], CdS/CdSe quantum dots[9,10] and perovskites[11] are employed as heterogeneous photocatalysts in conjunction with homogeneous Ni complexes for cross-couplings, they typically pose a risk of Ni contamination. Another approach involving immobilizing engineered Ni complexes containing carboxylic acid groups on the surface of dye or carbon dot sensitized $TiO_2$, which generally suffers from low stability[12,13]. In contrast, Ni single-atom incorporated graphite carbon nitride (g-$C_3N_4$) has emerged as a more efficient metallaphotocatalyst for cross-couplings, yet it faces challenges such as a low surface area for exposed catalytic sites, limited coordination sites and structural tunability, and restricted substrate functional diversity[14–18].

Covalent organic frameworks (COFs) represent a unique class of programable porous materials that allow the integration of diverse organic units into tailored semiconducting architectures[19–24]. Unlike other inorganic or organic semiconductors, COFs offer synthetically tunable topological structures and functions, with a precisely controlled chemical environment, achieved through the strategic selection of building blocks and linkage engineering[25–29]. By incorporating photoactive units with bipyridine- or phenanthroline-stabilized Ni single atoms in close proximity within COFs, the resulting metallaphotocatalysts exhibit superior catalytic activity compared to their Brownian motion-limited homogeneous counterparts (Fig. 1b)[30–36]. Notably, the linkages in COF-based dual metallaphotocatalysts play a crucial role by influencing the electron/energy transfer processes and framework stability. However, most COF-based metallaphotocatalysts are constructed from polarized imine or vinylene linkages, which are vulnerable to nucleophiles and radical species, thereby impairing electron and energy transfer dynamics[37]. In addition, reported COF-based metallaphotocatalysts typically employ specific bipyridine- or phenanthroline-derived monomers, limiting the ability to fine-tune the electronic structures of the metal centers. Furthermore, the chromophores commonly incorporated, such as Ir(bpy)(ppy)$_2$ (ppy = 2-phenylpyridine, bpy = 2,2′-bipyridine)[31], pyrene[33–35], and spirobifluorene[36], often suffer from restricted photoredox capabilities and suboptimal energy transfer properties. These limitations constrain the range of substrates and reaction patterns that can be effectively utilized in desired cross-coupling reactions. Therefore, there is a pressing need to develop tunable and robust COF-based metallaphotocatalysts capable of facilitating a broader spectrum of cross-coupling reactions.

Pyridyl-quinoline (PQ) ligands, developed by Li's group, form complexes with various transition metals, functioning as two-in-one metallaphotoredox catalysts to facilitate universal photocatalytic cross-couplings through intramolecular electron and energy transfer processes (Fig. 1c)[38]. Compared to dual-catalyst systems, this two-in-one system enhances reaction efficiency by positioning the metal centers near the formed radicals, thereby improving interactions between the substrate, photosensitizer, and metal center. However, despite the excellent advancements, these bifunctional metallaphotocatalysts

require high-energy light (390 nm) for activation, which can lead to substrate compatibility issues (e.g., dehalogenation of the aromatic halides). Additionally, they face challenges related to high metal loading and difficulties in catalyst separation and recycling.

We envisioned that integrating the PQ-ligated complex into fully conjugated and structurally stable COFs through deliberate linkage engineering would not only enable catalyst recycling and reuse but also broaden light absorption with improved catalytic activity. To achieve this, we designed COFs based on a novel three-in-one PQ-linkage that simultaneously functions as a structural connector, a photosensitizer and a metal-docking site. This multifunctional design facilitated the development of a series of PQ-linked COF-based metallaphotocatalysts capable of promoting universal cross-couplings between aromatic halides and diverse coupling partners (Fig. 1d). These PQ-linked COFs (PQCOFs) were modularly synthesized via trifluoromethanesulfonic acid (TfOH)-promoted three-component Povarov reactions involving tri-picolinaldehyde, tri-amines, and arylalkynes. These PQCOF-based metallaphotocatalysts, with nickel loading as low as 1 mol%, successfully facilitated the formation of a wide range of C($sp^2$)−X (X = S, N, O, C, B, P, Se, and Cl) bonds under visible-light irradiation. Importantly, the Ni-incorporated PQCOFs exhibited significantly enhanced catalytic activity compared to their homogeneous counterparts. These micrometer-sized catalysts demonstrated exceptional durability, being recyclable and reusable over 10 cycles while maintaining high catalytic efficiency with minimal metal leaching. The synthetic utility was highlighted by the application in the late-stage functionalization of pharmaceuticals, sequential functionalizations, and decagram-scale synthesis enabled by an in-house-built high-speed circulation flow system.

## Results

Bipyridine and phenanthroline are commonly utilized as building blocks in the construction of COFs to incorporate Ni single-atoms for cross-couplings[37]. However, these motifs typically lack inherent photoactivity and pose challenges in fine-tuning the electronic properties of the metal centers. Inspired by Li's system[38], we propose the introduction of an additional pyridine moiety adjacent to the quinoline group to create a bidentate pyridyl-quinoline (PQ) motif through rational linkage engineering. The unique PQ functionality fulfills a triple role: (i) acting as a chromophore for light harvesting, (ii) providing a bidentate binding site for metal incorporation, and (iii) serving as a robust linkage to prevent undesired reactions with nucleophiles and radicals, thereby enabling multifunctional metallaphotocatalysis.

To synthesize PQCOFs, we developed a three-component Povarov reaction utilizing strong-acidic TfOH as a catalyst under aerobic conditions[39,40]. We first achieved the model compound 4-(4-methoxyphenyl)-2-(pyridin-2-yl)quinoline (PQ-OMe) via a one-pot TfOH-catalyzed Povarov reaction involving picolinaldehyde, aniline, and 4-ethylnylanisole, thus verifying the feasibility of our three-component reaction strategy (Supplementary Fig. 3). In this reaction, TfOH catalyzes the imine condensation and promotes subsequent cycloaddition, while the presence of air facilitates aromatization to generate the fully conjugated quinoline ring. Based on this strategy, we conducted solvothermal reactions of 5,5′,5″-(benzene-1,3,5-triyl)tripicolinaldehyde (BTTPA), 1,3,5-tris[4-amino(1,1-biphenyl-4-yl)]benzene (TBA), and 4-ethylnylanisole in ethanol and mesitylene with TfOH as a catalyst at 120 °C under air for 3 days, resulting in PQCOF-OMe as a brown powder in 87% yield (Fig. 2a). Similarly, PQCOF-H and PQCOF-*t*Bu were synthesized under similar reaction conditions using phenylacetylene and 4-(*tert*-butyl)phenylacetylene as reactants, respectively (Supplementary Figs. 6 and 7). As a control experiment, the pyridyl-imine-linked COF named PICOF was prepared by the condensation of BTTPA and TBA using 9 M acetic acid as a catalyst (Fig. 2a). Our approach utilizes strong TfOH in combination with air as an oxidant, offering a more efficient and sustainable alternative to the conventional $BF_3$•$OEt_2$/DDQ or $B(C_6F_5)_3$/DDQ catalytic systems[41–45]. Notably, both the direct synthesis and post-synthetic modification using $BF_3$•$OEt_2$/DDQ have resulted in poorly crystalline or even non-crystalline products, underscoring the advantages of our protocol in achieving highly ordered structures (Supplementary Fig. 15).

The formation of the pyridyl-quinoline linkage in PQCOFs was investigated by a combination of Fourier transform infrared (FT-IR) spectroscopy, X-ray photoelectron spectroscopy (XPS), and solid-state cross-polarization magic-angle-spinning (CP-MAS) $^{13}$C NMR spectroscopy. In the FT-IR spectra of PQCOF-OMe, the strong characteristic peak at 1620 cm$^{-1}$, corresponding to the C = N stretching frequency of PICOF, disappeared, confirming the formation of the pyridyl-quinoline linkage (Fig. 2b). Additionally, the disappearance of the alkyne vibration frequencies at 3285 and 2106 cm$^{-1}$ and the appearance of the methoxy group frequency at 2837 cm$^{-1}$ further confirmed the formation of quinoline rings. XPS analyzes further support the formation of quinoline linkage. As shown in Supplementary Fig. 9, the N 1*s* peaks of PQCOF-OMe at 399.1 and 399.8 eV are associated with pyridine and quinoline nitrogen, respectively. This is distinct from PICOF, which has two N 1*s* peaks at 398.4 and 399.1 eV, corresponding to imine and pyridine nitrogen, respectively[46]. In the solid-state $^{13}$C CP/MAS NMR spectra, PICOF exhibited a characteristic imine peak at 157 ppm, which was absent in PQCOF-OMe (Fig. 2c). Instead, a peak corresponding to quinoline was observed at 159 ppm, along with a characteristic peak at 55 ppm assigned to the carbon of methoxy groups (Fig. 2c)[45], which further validated the successful formation of the pyridyl-quinoline linkages. Similar phenomena were also observed in the FT-IR spectra and solid-state CP-MAS $^{13}$C NMR of PQCOF-H and PQCOF-*t*Bu (Supplementary Figs. 8 and 10), indicating the universality of the one-pot protocol in forming the pyridyl-quinoline linkage in COFs.

The crystal structures of PQCOFs and PICOF were elucidated using powder X-ray diffraction (PXRD) analyzes. As shown in Fig. 2d, the PXRD pattern of PQCOF-OMe exhibited five prominent diffraction peaks, with the most intensive one at 3.20°, and the four other peaks at 5.50, 6.33, 8.39, and 25.05° assigned to the (100), (110), (200), (210), and (001) facets, respectively. In contrast, the PXRD of PICOF showed five peaks at 3.15, 5.43, 6.30, 8.27, and 24.39° which correspond to its (100), (110), (200), (210), (220) and (001) facets, respectively. The upshift of the main peak from 3.15 to 3.20° also confirmed the successful introduction of aromatic substituents (Supplementary Fig. 13). The Pawley refinement showed a good match with the experimental PXRD patterns of PICOF and PQCOF-OMe, with profile and weighted profile values of 4.35 and 5.83%, 3.34 and 4.18%, respectively. PICOF adopts AA stacking mode with refined cell parameters of $a = b =$ 33.64 Å, $c = 3.65$ Å, $\alpha = \beta = 90°$ and $\gamma = 120°$ (Figs. 2d and Supplementary Fig. 25). PQCOF-OMe also adopts an AA stacking with unit cell of $a = b = 32.89$ Å, $c = 3.83$ Å, $\alpha = \beta = 90°$ and $\gamma = 120°$ (Figs. 2d and Supplementary Fig. 26). Similarly, PQCOF-H and PQCOF-*t*Bu also displayed similar hexagonal lattices (Supplementary Figs. 27 and 28). Nitrogen sorption experiments at 77 K were conducted to evaluate the porosity of PQCOFs (Figs. 2e and Supplementary Figs. 16–19). The Brunauer-Emmett-Teller (BET) surface areas were estimated to be 1278, 1149, and 1081 m$^2$/g for PQCOF-OMe, PQCOF-H and PQCOF-*t*Bu, respectively. As illustrated in Supplementary Fig. 12, the SEM images of COFs reveal irregular block-like structures composed of small and dense particles with an average size of ~20 μm.

The Ni-incorporated COFs were facilely obtained by immersing PQCOFs into a DMA solution of $NiCl_2$·glyme (Fig. 3a). Inductively coupled plasma-optical emission spectroscopy (ICP-OES) was employed to precisely quantify the Ni content, which was measured to be 10.16%, 9.38%, and 9.10% by weight for Ni@PQCOF-OMe, Ni@PQCOF-H, and Ni@PQCOF-*t*Bu, respectively (Fig. 3a). The corresponding Ni-to-pyridyl-quinoline molar ratios were calculated to be 1.02, 0.89 and 0.94 for Ni@PQCOF-OMe, Ni@PQCOF-H, and Ni@PQCOF-*t*Bu, respectively, confirming that almost all the pyridyl-quinoline groups

https://doi.org/10.1038/s41467-025-59541-4

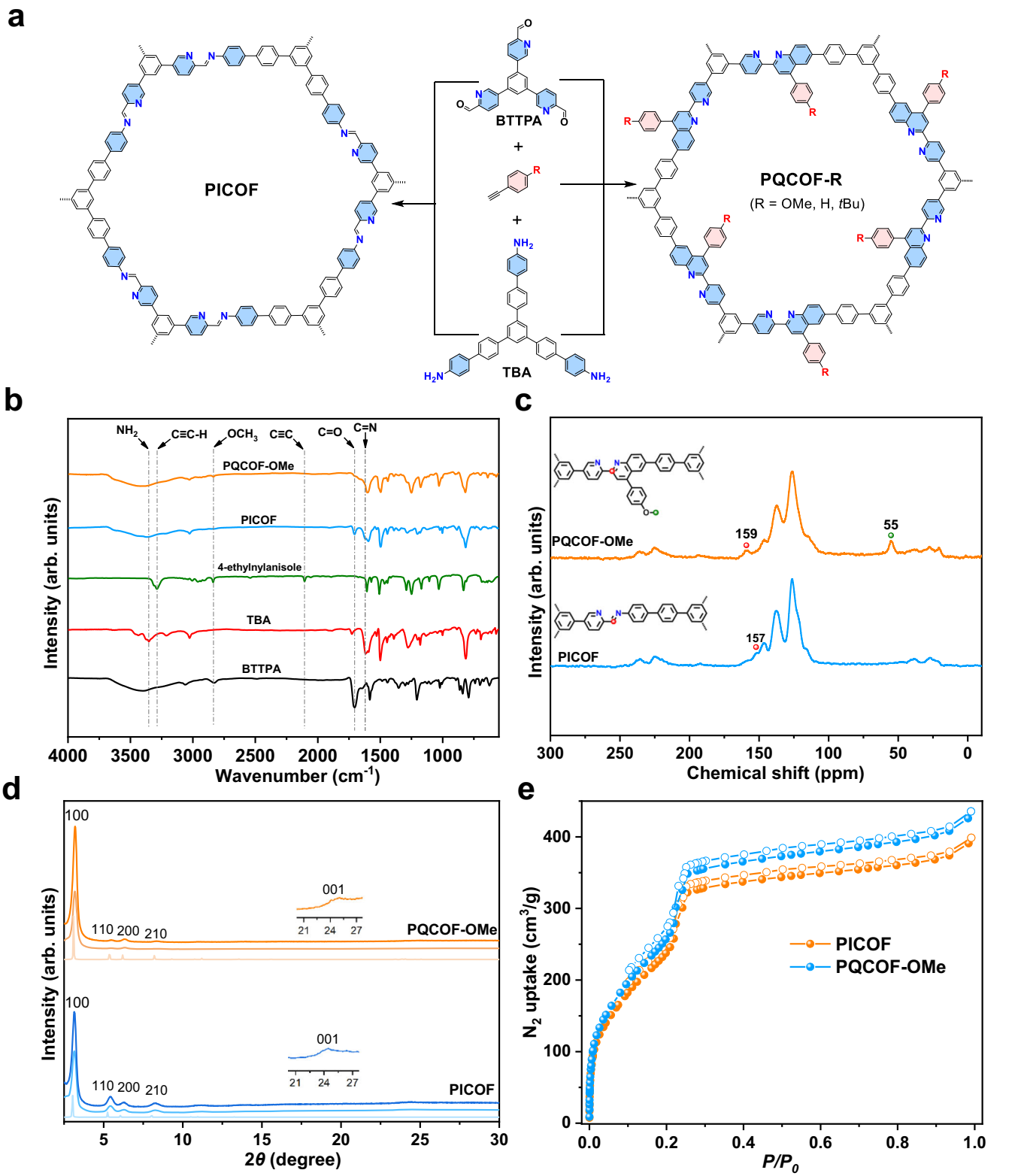


**Fig. 2 | Synthesis and characterization of COFs. a** Synthesis of PICOF and PQCOFs. **b** FT-IR spectra of PQCOF-OMe, PICOF and corresponding monomers. **c** Solid-state $^{13}C$ CP/MAS NMR spectrum of PQCOF-OMe and PICOF. **d** PXRD characterizations of PICOF (blue) and PQCOF-OMe (yellow). Each set of lines from top to bottom show experimental, Pawley-refined and simulated AA stacking PXRD patterns, respectively. The zoomed-in experimental PXRD patterns show the (001) peaks. **e** Nitrogen adsorption isotherms of PQCOF-OMe and PICOF.

are coordinated to Ni. The FT-IR spectra and solid-state $^{13}C$ CP/MAS NMR of Ni@PQCOF-OMe showed no perceptible change compared to PQCOF-OMe, revealing the retention of the backbone during the post-modification process (Supplementary Figs. 8 and 10). Moreover, the PXRD pattern of Ni@PQCOF-OMe remained similar to that of PQCOF-OMe, indicating that the crystallinity was well preserved (Supplementary Fig. 14). The BET surface area of Ni@PQCOF-OMe was determined to be 1098 $m^2/g$ (Fig. 5e).

https://doi.org/10.1038/s41467-025-59541-4

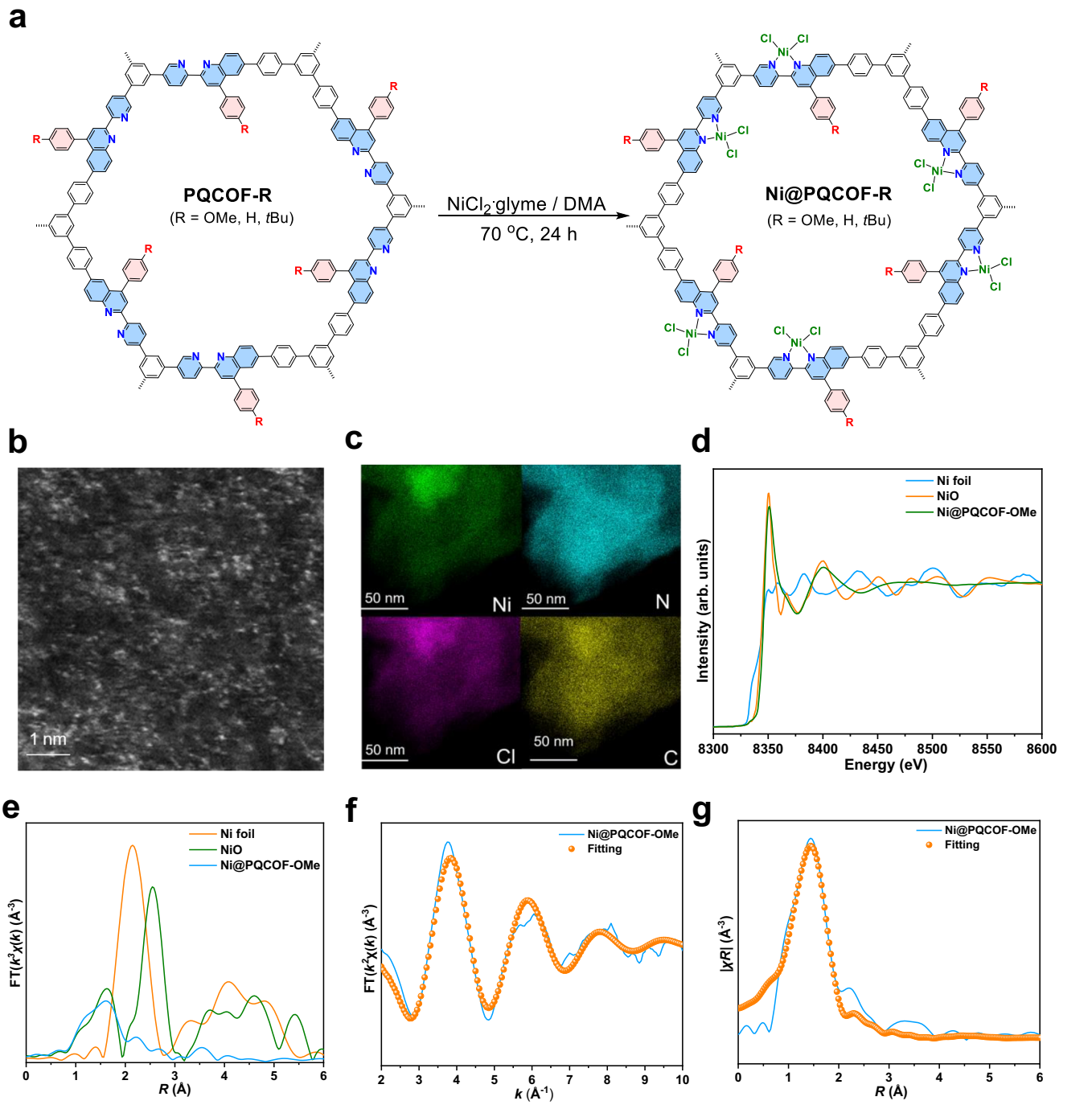


**Fig. 3 | Characterization of Ni single-atom incorporated PQCOF-OMe.** **a** Illustration of the incorporation of Ni single-atom into PQCOF-OMe. **b** HADD-STEM image of the atomically dispersed Ni in Ni@PQCOF-OMe. **c** TEM EDS-mapping of Ni, N, Cl, and C inside Ni@PQCOF-OMe; **d** XANEs curves of Ni@PQCOF-OMe. **e**–**g** EXAFS and fitting curves of Ni@PQCOF-OMe.

To confirm well dispersion of the single-atom Ni atoms in the framework, high-angle annular dark-field scanning transmission electron microscopy (HAADF-STEM) analysis was performed. As shown in Fig. 3b, bright spots corresponding to single Ni atoms with size of ~ 0.2 nm were uniformly distributed across the framework, with no evidence of Ni clusters or nanoparticles. Energy-dispersive X-ray (EDX) mapping further confirmed the uniform distribution of Ni, N, Cl, and C across all samples (Fig. 3c). Furthermore, X-ray absorption spectroscopy (XAS) was utilized to elucidate the electronic structure and local environment of the isolated Ni atoms. The Ni K-edge X-ray absorption near-edge structure (XANES) spectrum of Ni@PQCOF-OMe was shown in Fig. 3d, with Ni foil and NiO as references. The absorption edge position of Ni@PQCOF-OMe closely matched NiO rather than Ni foil, indicating that the Ni in the as-prepared Ni@PQCOF-OMe sample was in a valence state of +2 rather than a metallic one. Detailed structural information was obtained from the Fourier transform extended X-ray absorption fine structure (FT-EXAFS) spectra. As shown in Fig. 3d, the *R*-space spectrum of Ni@PQCOF-OMe displayed a distinct peak at around 1.6 Å, in accordance with the first coordination shell of Ni-N, and the peak of Ni-Ni at about 2.2 Å cannot be observed, suggesting that the Ni sites in Ni@PQCOF-OMe were atomically dispersed. Quantitative EXAFS analysis was conducted to analyze structure

parameters (Fig. 3e, f). The related fitting data of EXAFS are displayed in Supplementary Table 2. These results illustrate that Ni toms are confined in the COF host and are bonded with two N atoms with an atom distance of 1.79 and 1.86 Å (Ni-N) and two Cl atoms with an atom distance of 2.11 Å (Ni-Cl). Taken together, we confirmed the existence of the atomically dispersed Ni atoms in the COF backbone.

The UV-Vis diffuse reflectance spectra of PQCOFs show broader absorption compared to PICOF, which can be attributed to the increased π delocalization of the quinoline units (Supplementary Fig. 21). After the incorporation of Ni ions, the generated Ni@PQCOF-OMe shows an absorption edge at ~900 nm, indicating efficient visible-light absorption of the material. To examine the charge migration dynamics, steady-state photoluminescence spectra were recorded for PQCOF-OMe and Ni@PQCOF-OMe. As shown in Supplementary Fig. 22, Ni@PQCOF-OMe exhibits significantly decreased fluorescence intensity compared to PQCOF-OMe, suggesting efficient electron transfer or energy transfer from the COF backbone to Ni(II), resulting in the Ni(I) or excited Ni(II) species. Moreover, the shorter photoluminescence lifetime ($\tau = 2.93$ ns for Ni@PQCOF-OMe vs $\tau = 3.52$ ns for PQCOF-OMe, Supplementary Fig. 23) and stronger photocurrent responses further (Supplementary Fig. 24) further indicate enhanced electron-hole separation and increased charge transfer efficiency.

## Performance in photocatalytic cross-coupling reactions

Compared to conventional transition-metal promoted cross-couplings, photocatalytic cross-coupling reactions have significantly extended the reaction scope for carbon-carbon and carbon-heteroatom bond formations[47–50]. Benefited from the integrated multifunctionalities and excellent visible light absorption capacity, we speculated that the Ni single-atom incorporated PQCOFs could serve as highly effective heterogeneous metallaphotocatalysts for promoting visible-light-mediated cross-coupling reactions.

To verify our hypothesis, several representative and synthetic useful carbon-heteroatom bond formation reactions between aryl halides and coupling partners were examined. Initially, we tested the photocatalytic C–S coupling using methyl 4-iodobenzoate and ethyl 3-mercaptopropanoate as model substrates. After a systemic survey of various reaction parameters, we established a procedure that achieved the desired C–S coupling product (**1**) in 95% yield using 1 mol% Ni@PQCOF-OMe as the catalyst, $^{i}Pr_2NH$ as a base, and MeCN as the solvent under 456 nm light irradiation. As shown in Supplementary Table 4, our evaluation revealed that the photocatalyst, light, and base additives were all crucial for the transformation. Ni@PQCOF-OMe exhibited higher catalytic activity than Ni@PQCOF-H and Ni@PQCOF-*t*Bu, underscoring the importance of the electronic properties of the nickel sites on catalytic performance (entries 12 and 13, Supplementary Table 4). For comparison, Ni@PICOF showed significantly lower yield in C–S coupling (entry 15, Supplementary Table 4). Additionally, we synthesized a non-crystalline Ni@PQCOF-OMe, which exhibited a significantly lower yield compared to its crystalline counterpart (entry 14, Supplementary Table 4), suggesting the importance of crystallinity in enhancing the catalytic performance.

After identifying Ni@PQCOF-OMe as the most effective metallaphotocatalyst, we evaluated various aromatic halides to assess the scope of photocatalytic C($sp^2$)–S coupling reaction. Aryl halides with electronically biased substituents underwent smooth C–S couplings, giving thioethers **1-3** with up to 95% yield (Fig. 4). Moreover, a range of thiols including aliphatic thiols and thiophenol, were well tolerated to generate the corresponding products (**4-8**) in high efficiency. Sulfinates also served as effective coupling partners to generate sulfones **9** and **10** in high yields.

We then explored the broader catalytic potential of Ni@PQCOF-OMe for other carbon-heteroatom bond formations. A diverse array of N-, O-, B-, P-, Se-, and Cl-containing weak nucleophiles were effectively coupled. Using DABCO as the organic base, alkyl amines were coupled with aryl iodides to produce aryl amines (**11-18**) in good to excellent yields (Fig. 4). Aromatic amines and sulfonamide also delivered the target products (**19, 20**) efficiently. With TMG as the organic base, various O-containing partners, including alcohols and water, were effectively coupled to generate the corresponding ethers and phenol (**21-28**). Carboxylic acids proved to be competent coupling partners, delivering esters (**29** and **30**) in good yields using $Cs_2CO_3$ as the base. Additionally, C–B and C–P couplings were successfully achieved, producing aryl boric esters and phosphine oxides (**31-34**). Selenol and chloride ions could also be employed as coupling partners to afford the corresponding unsymmetric diphenyl selenides (**35, 36**) and phenyl chlorides (**37, 38**) in excellent yields.

Beyond carbon-heteroatom cross-couplings, Ni@PQCOF-OMe effectively catalyzed a wide range of carbon-carbon bond formation reactions. Alkyltrifluoroborates were employed for C($sp^2$)–C($sp^3$) couplings with various aromatic halides to efficiently deliver diarylmethanes (**39-42**) (Fig. 4). Additionally, phenylhydrazines were used for C($sp^2$)–C($sp^2$) cross-couplings, producing biphenyl compounds (**43-46**). Furthermore, aryl halides and phenylacetylenes underwent smooth C($sp^2$)–C($sp$) couplings to generate the desired coupling products (**47, 48**).

## Synthetic applications and circulation-flow enabled decagram-scale synthesis

The synthetic applicability of Ni@PQCOF-OMe-based heterogeneous metallaphotocatalytic cross-couplings was investigated for the late-stage diversification of bioactive and pharmaceutical molecules. As depicted in Fig. 5a, natural α-amino acid derivatives such as N-Boc-*L*-cysteine methyl ester and carbohydrate alcohols derived from *D*-fructose were amenable to the C–S and C–O couplings, yielding the corresponding products (**49, 50**) with high efficiency. Furthermore, drugs such as tryptamine and celecoxib served as coupling partners to produce the C–N coupling products (**51, 52**) in good yields. To further showcase the synthetic utility of our developed protocol, we applied it to the preparation of various drugs and drug intermediates, including intermediates for biphenamol (**53**), cefapirin (**54**), lorpiprazole (**55**), as well as the pharmaceuticals fluoxetine (**56**), paracetamol (**57**), and antifungal phosphonate (**58**) (Fig. 5b).

To enhance molecular complexity and achieve the controlled construction of a diverse compound library, we utilized Ni@PQCOF-OMe as a metallaphotocatalyst to facilitate the sequential difunctionalization of arenes via carbon-heteroatom or carbon-carbon cross-coupling reactions[51,52]. By exploiting the preferential reactivity of aryl iodo groups over bromo groups and carefully controlling the feeding ratio of nucleophiles, we successfully carried out C-S, C-N, C-O, and C-C couplings in varying sequences using thiols, sulfinates, water, amines, and potassium benzyltrifluoroborates as nucleophiles (Fig. 5c). The Ni@PQCOF-OMe-catalyzed sequential transformations accessed difunctionalized arenes (**59-66**) with generally good overall yields, offering a versatile approach to introduce functionalities to arenes in a customizable manner.

In addition, we employed a simple in-house-built high-speed circulation flow system for decagram-scale synthesis through Ni@PQCOF-OMe-based heterogeneous photocatalysis (Fig. 5d and Supplementary Fig. 29)[53,54]. With this system, we performed the photocatalytic cross-coupling between methyl 4-bromobenzoate and ethyl 3-mercaptopropanoate at a 50 mmol scale, resulting in the corresponding C-S coupling product with an isolated yield of 86%. In another example, the cross-coupling of methyl 4-iodobenzoate with piperidine proceeded smoothly, yielding the target C-N coupling product with an 83% yield. These results highlight the efficiency and practical utility of the high-speed circulation flow reactor for scaling up heterogeneous photocatalysis.

https://doi.org/10.1038/s41467-025-59541-4

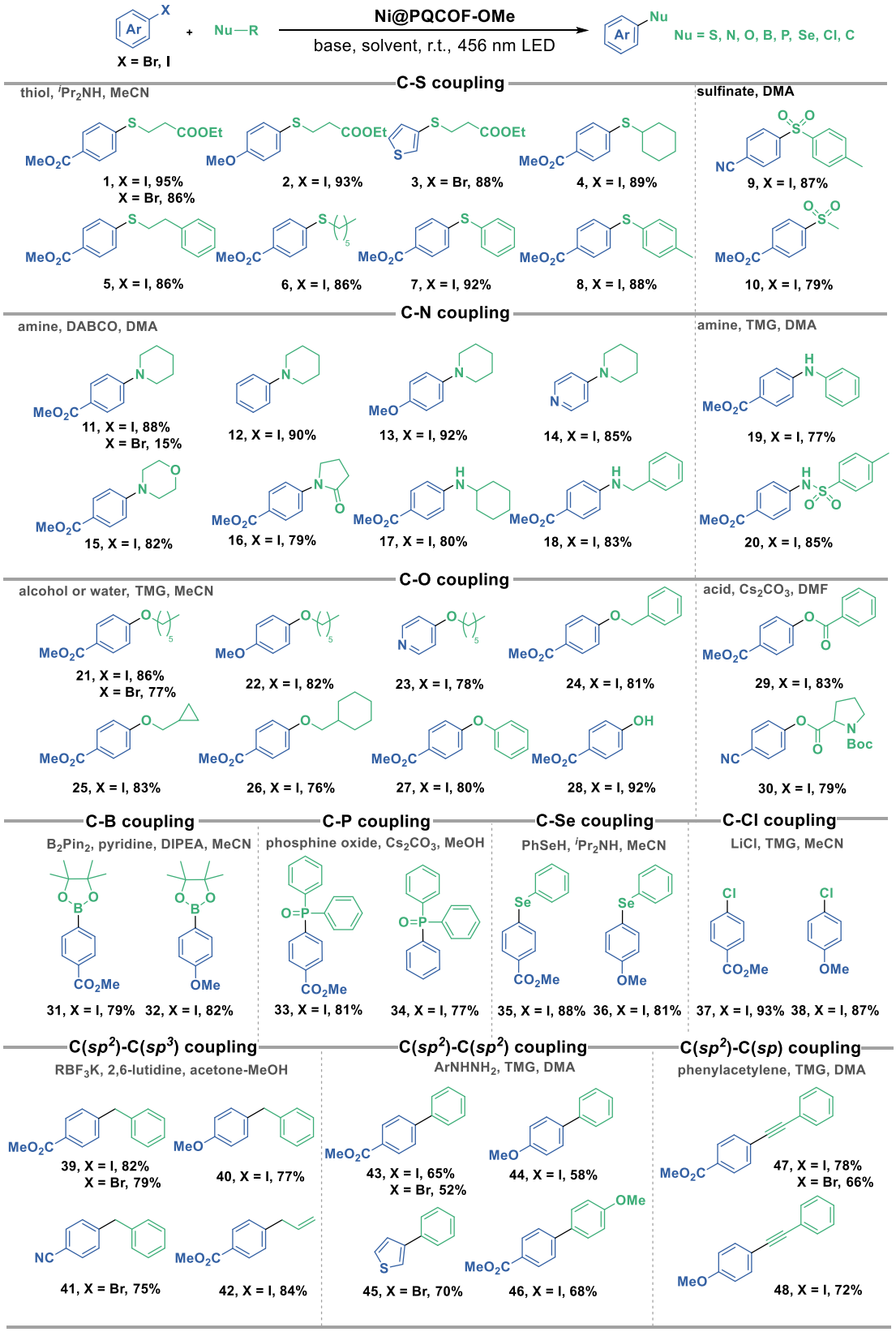


**Fig. 4** | Ni@PQCOF-OMe promoted cross-couplings under visible-light irradiation, including C–S, C–N, C–O, C–B, C–P, C–Se, C–Cl, and C–C couplings.

## Distinct advantages, recyclability, and stability of COF-based metallaphotocatalysts

To highlight the advantages of our heterogeneous photocatalysts, we compared the catalytic activity of Ni@PQCOF-OMe with its homogeneous counterpart, $Ni^{2+}$/PQ-OMe. We employed 390 nm light for the homogeneous photocatalyst, as its absorption significantly decreases above 400 nm, while Ni@PQCOF-OMe was activated by 456 nm light, benefiting from its extended absorption range due to the

https://doi.org/10.1038/s41467-025-59541-4

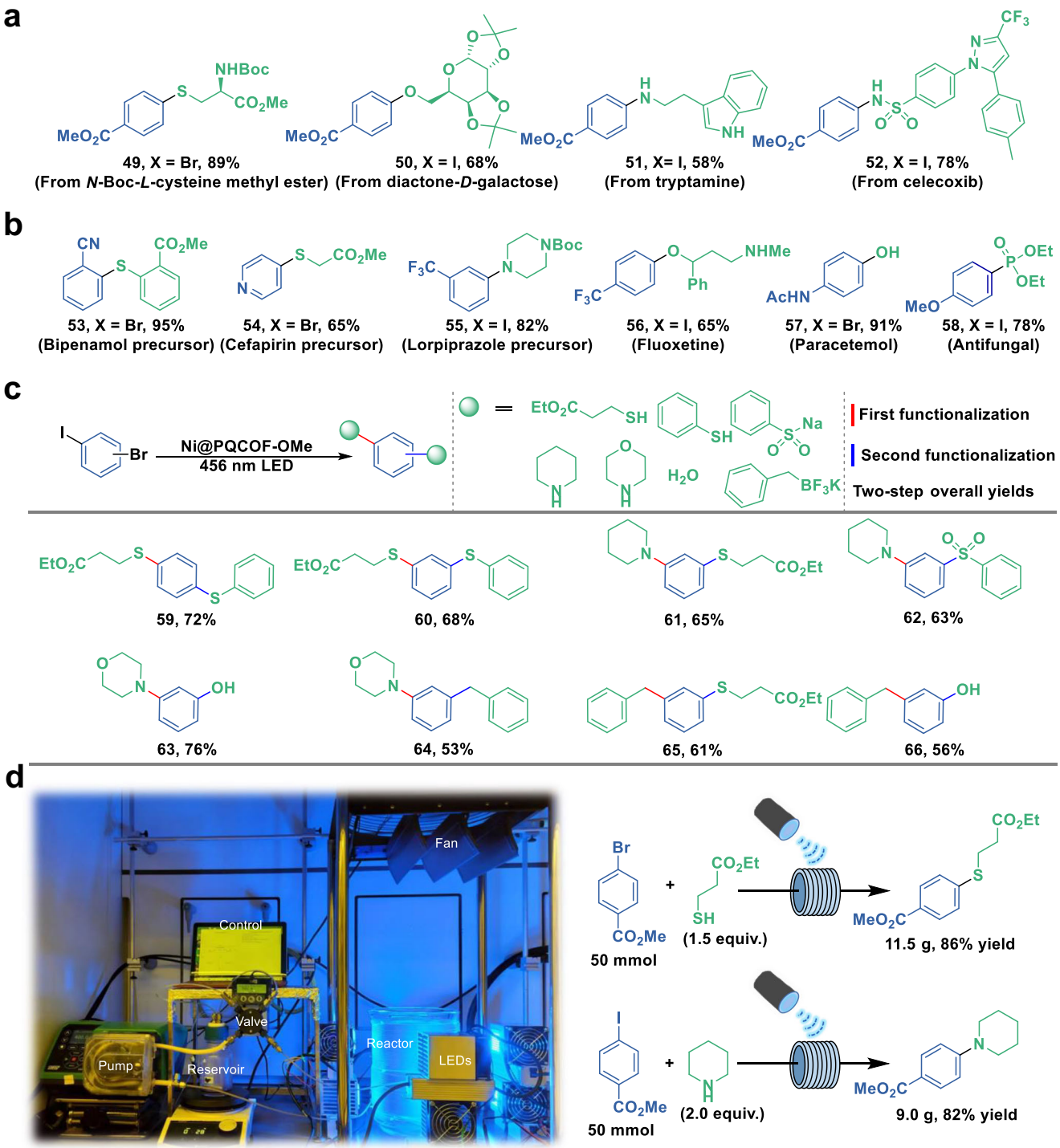


**Fig. 5 | Further synthetic utility of Ni@PQCOF-OMe mediated photocatalytic cross-couplings. a** Late-stage functionalization of diverse bioactive molecules. **b** Synthesis of drugs and drug precursors. **c** Sequential cross-couplings enabled by Ni@PQCOF-OMe mediated photocatalysis. **d** High-speed circulation-flow enabled decagram-scale synthesis.

conjugated COF structure (Fig. 6a). At the same Ni loading, Ni@PQ-COF-OMe exhibited a 3-7-fold enhancement in catalytic efficiency compared to $Ni^{2+}$/PQ-OMe (Fig. 6b). Notably, in the C–S cross-coupling reaction, Ni@PQCOF-OMe achieved an impressive 95% yield, whereas the homogeneous $Ni^{2+}$/PQ-OMe system was ineffective. Furthermore, the calculated quantum yields were 0.012 for $Ni^{2+}$/PQ-OMe and 0.060 for Ni@PQCOF-OMe, highlighting the superior photon utilization efficiency of the heterogeneous system. The superior catalytic activity of Ni@PQCOF-OMe can be attributed to several key factors. First, homogeneous systems require high-energy light (390 nm) for activation, which often lead to undesired dehalogenation of aromatic halides, resulting in reduced coupling yields (Supplementary Fig. 30). In contrast, Ni@PQCOF-OMe benefits from an extended absorption range due to its conjugated COF structure, enabling more efficient light harvesting to absorb visible light. Additionally, homogeneous systems suffer from nickel deactivation via aggregation into nickel nanoparticles (nickel black), necessitating a high metal loading to maintain catalytic activity (Supplementary Fig. 31). The rigid and

https://doi.org/10.1038/s41467-025-59541-4

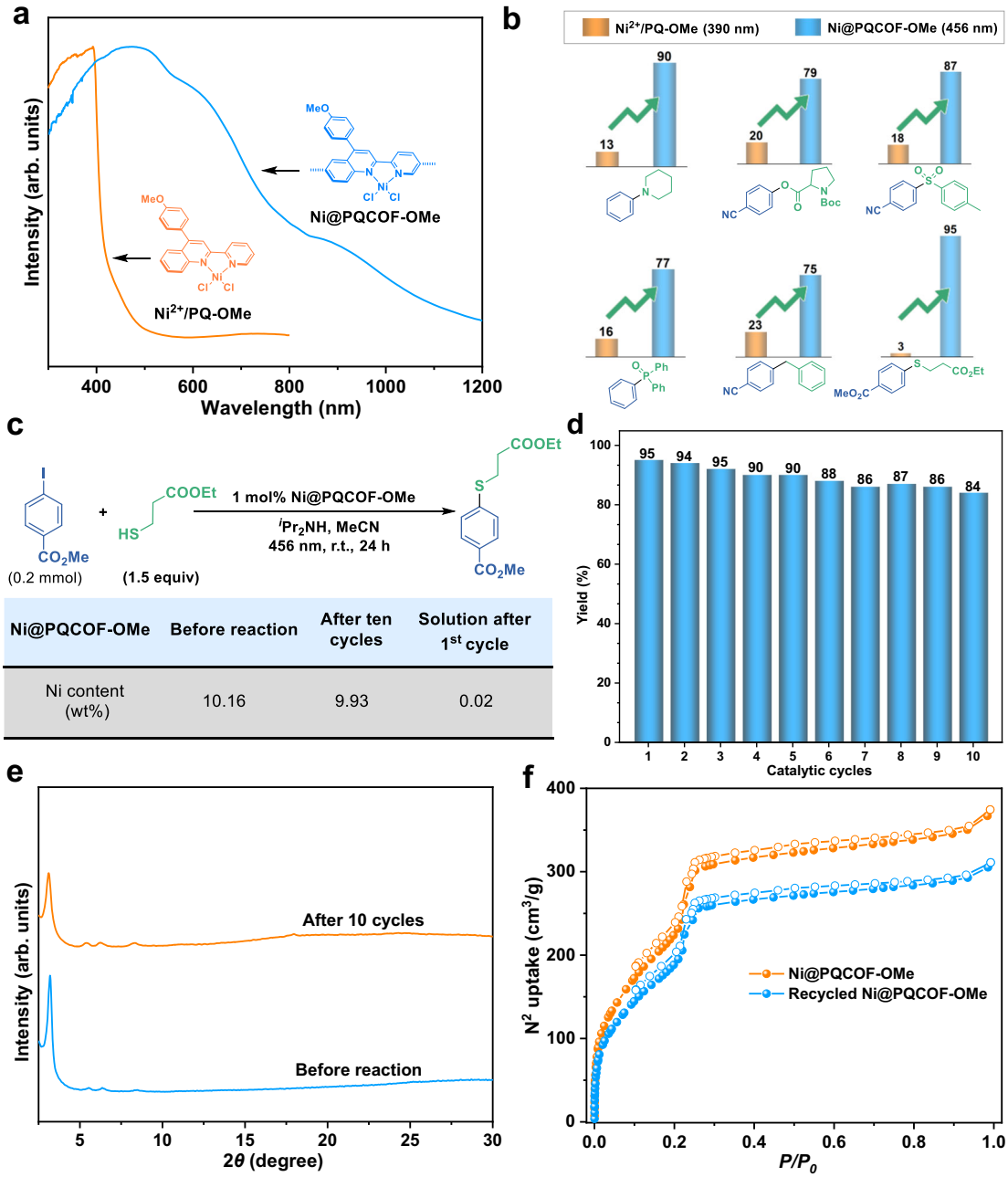


| Ni@PQCOF-OMe | Before reaction | After ten cycles | Solution after 1st cycle |
|---|---|---|---|
| Ni content (wt%) | 10.16 | 9.93 | 0.02 |

**Fig. 6 | Catalytic activity comparison and recyclability test. a** Comparison of the UV-Vis spectra for Ni@PQCOF-OMe and $Ni^{2+}$/PQ-OMe. **b** Catalytic performance comparison of Ni@PQCOF-OMe-based metallaphotocatalyst and $Ni^{2+}$/PQ-OMe homogeneous catalytic system. **c**, **d** Metal leaching test and recycling results for heterogeneous photocatalytic cross-coupling of methyl 4-iodobenzoate and ethyl 3-mercaptopropanoate. **e** PXRD patterns and (**f**) nitrogen adsorption isotherms for the recycled and original Ni@PQCOF-OMe.

porous COF framework in Ni@PQCOF-OMe prevents metal leaching and aggregation, ensuring long-term catalyst stability. Furthermore, the confined coordination environment within the COF enhances charge separation and electron transfer, reducing the possibility of catalyst deactivation. Therefore, the heterogenization of the PQ-ligated nickel complex not only enhances catalyst stability but also improves substrate tolerance by minimizing side reactions and maintaining a high density of active Ni sites.

Compared to previously reported COF-based metallaphotocatalysts, our three-in-one catalytic system presents several distinct advantages. First, while existing COF-based metallaphotocatalysts have exhibited high activity in diverse cross-couplings, they are limited in scope. For instance, Ni@$sp^2$c-COF can support five types of cross-couplings but shows low catalytic activity towards the C($sp^2$)-N couplings between aromatic halides and amines[36] and lacks the ability to catalyze C($sp^2$)-C couplings (Supplementary Fig. 32). In contrast, our Ni-PQCOFs facilitate eight distinct cross-coupling reactions, including C($sp^2$)−C couplings, representing the broadest range of cross-coupling achieved to date. Second, imine-conjugated imine-linked metallaphotocatalysts are prone to degradation in the presence of nucleophiles due to exchange reactions, and cyano-substituted olefin linkages are susceptible to radical attacks. Our PQ linkage, however, features fully conjugated structures that resist nucleophile exchange and radical addition, ensuring enhanced stability. Third, unlike conventional metallaphotocatalytic systems that rely on electron/energy transfer between chromophores and nickel sites, our three-in-one system

leverages chromophores as linkages directly coordinated to the nickel center, resulting in superior catalytic efficiency. Additionally, our COF-based metallaphotocatalyst can perform sequential difunctionalization of arenes, highlighting its enhanced versatility in synthetic applications.

A further key advantage of using heterogeneous catalysts lies in their recoverability and reusability. The micrometer-sized Ni@PQCOF-OMe catalyst could be easily separated and recycled from the reaction mixture through direct filtration (Supplementary Figs. 33a and 33b). As shown in Fig. 6d, Ni@PQCOF-OMe were recovered and reused for at least ten cycles to produce the C–S coupling product **1** without a significant decrease in yield. Additionally, negligible leaching of $Ni^{2+}$ (0.02 wt%) was detected during the recycling process (Fig. 6c). PXRD measurements and nitrogen adsorption isotherms of the original and recovered Ni@PQCOF-OMe samples indicated that the crystalline porous structure was maintained during photocatalysis (Fig. 6e, f). Furthermore, the catalyst's robustness was demonstrated by comparing the UV-Vis spectra and FT-IR spectra of the recovered and original Ni@PQCOF-OMe after the photocatalytic C–S coupling reaction (Supplementary Figs. 33c and 33d).

## Discussion

In summary, we have designed and synthesized a class of three-in-one Ni-PQCOF photocatalysts through Brønsted-acid-promoted Povarov reactions, where the (photo)chemically stable PQ-linkage was introduced as a chromophore and a metal-binding ligand, thereby significantly broadening the scope of multifunctional COF metallaphotocatalysts. Ni-PQCOFs serve as a universal photocatalytic platform for C($sp^2$)–(hetero)atom (S, N, O, C, B, P, Se, and Cl) cross-coupling reactions. These fully conjugated PQCOF catalysts not only deliver generally improved yields, but also enable transformations previously unattainable with homogeneous counterparts, owing to their extended absorption and exceptional (photo)chemical stability. Their applications extend to late-stage functionalization of pharmaceutical molecules, sequential functionalizations, and large-scale flow synthesis. Moreover, these catalysts exhibit excellent recyclability, maintaining high activity over ten cycles with minimal metal leaching. The modular structural scaffolds, capability to incorporate various metal centers, superiority over homogeneous systems, along with the facile integration of additional functions into the three-in-one PQCOF platform, collectively pave the way for the development of more powerful multifunctional metallaphotocatalysts.

## Methods

### Synthesis of PQCOF-OMe

To a 10 mL Schlenk tube was added with BTTPA (20 mg, 0.05 mmol), TBA (30 mg, 0.05 mmol), 1-ethynyl-4-methoxybenzene (39 µL, 0.30 mmol), mesitylene (0.5 mL) and EtOH (0.5 mL). The mixture was sonicated for 2 mins and added with 0.2 M TfOH solution (100 µL). The tube was then sealed and heated at 120 °C in an oven for three days. The solid obtained was washed with THF 3 times and dried under vacuum to afford a brown solid in 87% yield.

### Synthesis of Ni@PQCOF-OMe

50 mg PQCOF-OMe was treated with $NiCl_2$·glyme (30 mg) in 5 mL DMA. The mixture was heated at 60 °C and stirred for 24 h. After reaction, the resulting solid was filtered, washed with DMF and methanol three times each, and dried under vacuum at 120 °C overnight to yield the desired Ni@PQCOF-OMe.

### General procedure for photocatalytic C-S coupling reaction of aromatic halides and thiols

To a 10 mL oven-dried sealed tube equipped with a magnetic stir bar was added the corresponding aryl halide (0.2 mmol), thiol (0.3 mmol), and Ni@PQCOF-OMe (1 mol% Ni). Then, dry MeCN (1 mL) and $^iPr_2NH$ (0.6 mmol) were added. The tube was sealed with a rubber septum and the reaction mixture was degassed by three cycles vacuum/argon of "freeze-pump-thaw". The reaction mixture was then stirred and irradiated by blue LEDs (30 W, 456 nm) for 24 h. A fan was used to maintain the temperature. After that, the reaction mixture was removed from the light source and diluted with 5 mL of $CH_2Cl_2$. The filtrate was concentrated, and the residue was purified by column chromatography over silica gel or prepared-TLC to give the corresponding products.

### Recycling test

To a 10 mL oven-dried sealed tube equipped with a magnetic stir bar was added methyl 4-iodobenzoate and (0.4 mmol, 104.8 mg), ethyl 3-mercaptopropanoate (0.6 mmol, 76 µL), and Ni@PQCOF-OMe (1 mol% Ni). Then, dry MeCN (2 mL) and $^iPr_2NH$ (1.2 mmol, 168 µL) were added. The tube was sealed with a rubber septum and the reaction mixture was degassed by three cycles vacuum/argon of "freeze-pump-thaw". The reaction mixture was then stirred and irradiated by blue LEDs (30 W, 456 nm) for 24 h. A fan was used to maintain the temperature. After that, the reaction mixture was removed from the light source and diluted with 10 mL of $CH_2Cl_2$. The filtrate was concentrated, and the residue was purified by column chromatography over silica gel to give product **1**. While the catalyst was washed with DMF and acetone three times and dried at 80 °C for 12 h before the next reaction cycle.

### High-speed circulation-flow enabled decagram-scale synthesis

To a Duran® screwed bottle (volume = 500 mL) was added MeCN (200 mL), Ni@PQCOF-OMe (1 mol%), methyl 4-bromobenzoate (50 mmol, 10.9 g), ethyl 3-mercaptopropanoate (75 mmol, 9.5 mL), and $^iPr_2NH$ (150 mmol, 21.2 mL) successively. Under stirring, the resulted slurry was bubbled with argon for 30 min. The slurry mixture was subjected to ultrasonication for 10 min, which was ready for use. After pretreatment, the tubing system was purged with argon for 20 min, then connected to the Duran® bottle containing the reaction mixture under argon protection. The pump was started with the set flow rate (300 mL/min). Once the tubing was filled with the reaction mixture, the two-way valve was adjusted to allow the slurry to circulate within the tubing reactor. Then, with eye protection, all LEDs were turned on (tubing volume: 250 mL; solvent volume: 60 mL; LED lights: 4 sets, 60 W/set, 455 nm). After 24 h, all LEDs and the cooling systems were switched off. The reaction mixture in the tubing and the Duran® bottle was transferred into a 250 mL flask. The tubing and the bottle were washed with 200 mL $CH_2Cl_2$. The filtrate was concentrated, and the residue was purified by column chromatography over silica gel to give product **1**.

## Data availability

The X-ray crystallographic coordinates for structures reported in this article have been deposited at the Cambridge Crystallographic Data Center (CCDC), under deposition numbers CCDC 2363625. These data can be obtained free of charge from the CCDC via www.ccdc.cam.ac.uk/data_request/cif. All data supporting the findings of this study are available within the article and the Supplementary Information file, or available from the corresponding authors upon request Source data are provided with this paper.

## References

1. Chan, A. Y. et al. Metallaphotoredox: the merger of photoredox and transition metal catalysis. *Chem. Rev.* **122**, 1485–1542 (2022).
2. Tasker, S. Z., Standley, E. A. & Jamison, T. F. Recent advances in homogeneous nickel catalysis. *Nature* **509**, 299–309 (2014).
3. Tellis, J. C. et al. Single-electron transmetalation via photoredox/nickel dual catalysis: unlocking a new paradigm for $sp^3$-$sp^2$ cross-coupling. *Acc. Chem. Res.* **49**, 1429–1439 (2016).

4. Diccianni, J., Lin, Q. & Diao, T. Mechanisms of nickel-catalyzed coupling reactions and applications in alkene functionalization. *Acc. Chem. Res.* **53**, 906–919 (2020).
5. Kariofillis, S. K. & Doyle, A. G. Synthetic and mechanistic implications of chlorine photoelimination in nickel/photoredox C($sp^3$)-H cross-coupling. *Acc. Chem. Res.* **54**, 988–1000 (2021).
6. Zhang, J. & Rueping, M. Metallaphotoredox catalysis for $sp^3$ C–H functionalizations through hydrogen atom transfer (HAT). *Chem. Soc. Rev.* **53**, 4099–4120 (2023).
7. Gisbertz, S., Reischauer, S. & Pieber, B. Overcoming limitations in dual photoredox/nickel-catalysed C–N cross-couplings due to catalyst deactivation. *Nat. Catal.* **3**, 611–620 (2020).
8. Zhao, Z., Pieber, B. & Delbianco, M. Modulating the surface and photophysical properties of carbon dots to access colloidal photocatalysts for cross-couplings. *ACS Catal.* **12**, 13831–13837 (2022).
9. Caputo, J. A. et al. General and efficient C–C bond forming photoredox catalysis with semiconductor quantum dots. *J. Am. Chem. Soc.* **139**, 4250–4253 (2017).
10. Liu, Y., Liang, D., Lu, L. & Xiao, W. Practical heterogeneous photoredox/nickel dual catalysis for C–N and C–O coupling reactions. *Chem. Commun.* **33**, 4853–4856 (2019).
11. Zhu, X. et al. Lead halide perovskites for photocatalytic organic synthesis. *Nat. Commun.* **10**, 2843 (2019).
12. Reischauer, S., Strauss, V. & Pieber, B. Modular, self-assembling metallaphotocatalyst for cross-couplings using the full visible-light spectrum. *ACS Catal.* **10**, 13269–13274 (2020).
13. Zhao, Z., Reischauer, S., Pieber, B. & Delbianco, M. Carbon dot/$TiO_2$ nanocomposites as photocatalysts for metallaphotocatalytic carbon–heteroatom cross-couplings. *Green Chem.* **23**, 4524–4530 (2021).
14. Ghosh, I. et al. Organic semiconductor photocatalyst can bifunctionalize arenes and heteroarenes. *Science* **365**, 360–366 (2019).
15. Bajada, M. A. et al. Light-driven C–O coupling of carboxylic acids and alkyl halides over a Ni single-atom catalyst. *Nat. Synth.* **2**, 1092–1103 (2023).
16. Xing, L. et al. Poly(heptazine imide) ligand exchange enables remarkable low catalyst loadings in heterogeneous metallaphotocatalysis. *Nat. Commun.* **14**, 1501 (2023).
17. Vijeta, A., Casadevall, C. & Reisner, E. An integrated carbon nitride-nickel photocatalyst for the amination of aryl halides using sodium azide. *Angew. Chem. Int. Ed.* **61**, e202203176 (2022).
18. Zhao, X. et al. Nickel-coordinated carbon nitride as a metallaphotoredox platform for the cross-coupling of aryl halides with alcohols. *ACS Catal.* **10**, 15178–15185 (2020).
19. Diercks, C. S. & Yaghi, O. M. The atom, the molecule, and the covalent organic framework. *Science* **355**, eaal1585 (2017).
20. Huang, N., Wang, P. & Jiang, D. Covalent organic frameworks: a materials platform for structural and functional designs. *Nat. Rev. Mater.* **1**, 16068 (2016).
21. Waller, P. J., Gandara, F. & Yaghi, O. M. Chemistry of covalent organic frameworks. *Acc. Chem. Res.* **48**, 3053–3063 (2015).
22. Wang, H. et al. Covalent organic framework photocatalysts: structures and applications. *Chem. Soc. Rev.* **49**, 4135–4165 (2020).
23. Chen, H. et al. Engineering covalent organic frameworks as heterogeneous photocatalysts for organic transformations. *Angew. Chem. Int. Ed.* **61**, e202204938 (2022).
24. Basak, A., Karak, S. & Banerjee, R. Covalent organic frameworks as porous pigments for photocatalytic metal-free C–H borylation. *J. Am. Chem. Soc.* **145**, 7592–7599 (2023).
25. Han, X. et al. Chiral covalent organic frameworks with high chemical stability for heterogeneous asymmetric catalysis. *J. Am. Chem. Soc.* **139**, 8693–8697 (2017).
26. Yuan, C. et al. Crystalline C—C and C=C bond-linked chiral covalent organic frameworks. *J. Am. Chem. Soc.* **143**, 369–381 (2021).
27. Qian, C. et al. Imine and imine-derived linkages in two-dimensional covalent organic frameworks. *Nat. Rev. Chem.* **6**, 881–898 (2022).
28. Li, X. et al. Constructing ambivalent imidazopyridinium-linked covalent organic frameworks. *Nat. Syn.* **1**, 382–392 (2022).
29. Wei, P.-F. et al. Benzoxazole-linked ultrastable covalent organic frameworks for photocatalysis. *J. Am. Chem. Soc.* **140**, 4623–4631 (2018).
30. Dong, J., Han, X., Liu, Y., Li, H. & Cui, Y. Metal–covalent organic frameworks (MCOFs): a bridge between metal–organic frameworks and covalent organic frameworks. *Angew. Chem. Int. Ed.* **59**, 13722–13733 (2020).
31. Jati, A. et al. Dual metalation in a two-dimensional covalent organic framework for photocatalytic C–N cross-coupling reactions. *J. Am. Chem. Soc.* **144**, 7822–7833 (2022).
32. Lopez-Magano, A. et al. Photoredox heterobimetallic dual catalysis using engineered covalent organic frameworks. *ACS Catal.* **11**, 12344–12354 (2021).
33. Fan, Y., Kang, D. W., Labalme, S., Li, J. & Lin, W. Enhanced energy transfer in a π-conjugated covalent organic framework facilitates excited-state nickel catalysis. *Angew. Chem. Int. Ed.* **62**, e202218908 (2023).
34. Jati, A., Dam, S., Kumar, S., Kumar, K. & Maji, B. A π-conjugated covalent organic framework enables interlocked nickel/photoredox catalysis for light-harvesting cross-coupling reactions. *Chem. Sci.* **14**, 8624–8634 (2023).
35. Hu, H.-C. et al. Bottom-up construction of Ni(II)-incorporated covalent organic framework for metallaphotoredox catalysis. *Chem. Eur. J.* **30**, e202303476 (2024).
36. Fan, Y., Kang, D. W., Labalme, S. & Lin, W. A spirobifluorene-based covalent organic framework for dual photoredox and nickel catalysis. *J. Am. Chem. Soc.* **145**, 25074–25079 (2023).
37. Jia, T., Zhao, Y., Song, W. & Zhao, J. Metallaphotocatalytic platforms based on covalent organic frameworks for cross-coupling reactions. *ChemCatChem* **16**, e202301522 (2024).
38. Li, J., Huang, C.-Y. & Li, C.-J. Two-in-one metallaphotoredox cross-couplings enabled by a photoactive ligand. *Chem* **8**, 2419–2431 (2022).
39. Laguna, E. M. et al. Structure and properties of neutral and cationic gold(III) complexes from substituted 2-(2′-pyridyl)quinoline ligands. *Inorg. Chem.* **53**, 12231–12233 (2014).
40. Zhang, X., Xu, X., Yu, L. & Zhao, Q. Three-component reactions of aldehydes, amines, and alkynes/alkenes catalyzed by trifluoromethanesulfonic acid: an efficient route to substituted quinolines. *Asian J. Org. Chem.* **3**, 281–284 (2014).
41. Li, X. et al. Facile transformation of imine covalent organic frameworks into ultrastable crystalline porous aromatic frameworks. *Nat. Commun.* **9**, 2998 (2018).
42. Li, X.-T. et al. Construction of covalent organic frameworks via three-component one-pot Strecker and Povarov reactions. *J. Am. Chem. Soc.* **142**, 6521–6526 (2020).
43. Das, P., Roeser, J. & Thomas, A. Solar light driven $H_2O_2$ production and selective oxidations using a covalent organic framework photocatalyst prepared by a multicomponent reaction. *Angew. Chem. Int. Ed.* **62**, e202304349 (2023).
44. Liu, H. et al. One-pot synthesis of fully-conjugated chemically stable two-dimensional covalent organic framework. *Chin. J. Chem.* **40**, 699–704 (2022).
45. Wang, J.-R. et al. Robust links in photoactive covalent organic frameworks enable effective photocatalytic reactions under harsh conditions. *Nat. Commun.* **15**, 1267 (2024).
46. Wu, W. et al. Pyridine-based covalent organic frameworks with pyridyl-imine structures for boosting photocatalytic $H_2O_2$ production via one-step $2e^-$ oxygen reduction. *Angew. Chem. Int. Ed.* **63**, e202404563 (2024).

47. Ghosh, I. et al. General cross-coupling reactions with adaptive dynamic homogeneous catalysis. *Nature* **619**, 87–93 (2023).
48. Zhu, C., Yue, H., Jia, J. & Rueping, M. Nickel-catalyzed c-heteroatom cross-coupling reactions under mild conditions via facilitated reductive elimination. *Angew. Chem. Int. Ed.* **60**, 17810–17831 (2021).
49. Zhu, S., Li, H., Li, Y., Huang, Z. & Chu, L. Exploring visible light for carbon–nitrogen and carbon–oxygen bond formation via nickel catalysis. *Org. Chem. Front.* **10**, 548–569 (2023).
50. Palowitz, M. D., Emmanuel, M. A. & Oderinde, M. S. A paradigm shift in catalysis: electro- and photomediated nickel-catalyzed cross-coupling reactions. *Acc. Chem. Res.* **56**, 2851–2865 (2023).
51. Duker, J., Ghosh, I. & Konig, B. Sequential one-pot (het)arene thioetherification and amination with nickel and visible light. *ACS Catal.* **13**, 13618–13625 (2023).
52. Cabrera-Afonso, M. J. et al. Engaging sulfinate salts via Ni/photoredox dual catalysis enables facile $Csp^2$–$SO_2R$ coupling. *Chem. Sci.* **9**, 3186–3191 (2018).
53. Liu, C. et al. High-speed circulation flow platform facilitating practical large-scale heteroegeneous photocatalysis. *Org. Process. Res. Dev.* **28**, 1964–1970 (2024).
54. Liu, T. et al. Modular assembly of arenes, ethylene and heteroarenes for the synthesis of 1,2-arylheteroaryl ethanes. *Nat. Chem.* **16**, 1705–1714 (2024).

## Acknowledgements

Jie W. acknowledges the financial support from the Prime Minister's Office of Singapore under its NRF-CRP Program (NRF-CRP29–2022-0004), the Agency for Science, Technology and Research (A*STAR) under its MTC IRG Grant (Project M22K2c0082), National Natural Science Foundation of China (22371200), the NUS (Suzhou) Research Institute, and the financial support from Pfizer (A-8002093-00-00).

## Author contributions

J.W. conceived and designed the program. H.J. designed and performed the experiments. W.Z. helped the substrate scope expansion. Jiale W. performed the high-speed circulation flow synthesis. Q.W. helped with the material synthesis and characterization. P.O'Neill and S.R.D. contributed to project discussion and data analysis. H.J., G.W. and J.W. wrote the paper. All authors discussed and commented on the final paper and contributed to the analysis and interpretation of the results.

## Competing interests

The authors declare no competing interests.

## Additional information

**Supplementary information** The online version contains supplementary material available at https://doi.org/10.1038/s41467-025-59541-4.

**Correspondence** and requests for materials should be addressed to Jie Wu.

**Peer review information** *Nature Communications* thanks the anonymous reviewers for their contribution to the peer review of this work. A peer review file is available.



**Hong Jiang[1], Weigang Zhang[1], Jiale Wu[1], Qijian Wang[1], Gan Wang[1], Patrick O'Neill[2], Srinivas Reddy Dubbaka[3] & Jie Wu[1]**

[1]Department of Chemistry, National University of Singapore, 3 Science Drive 3, Singapore, Singapore. [2]Pfizer Ireland Pharmaceuticals, Process Development Centre, Ringaskiddy (PDC), Co-Cork, Ireland. [3]Pfizer Asia Manufacturing Pte Ltd, Singapore, Singapore. e-mail: chmjie@nus.edu.sg